Near-field radiative heat transfer between macroscopic planar surfaces

Richard Ottens,[1] V. Quetschke,[2] Stacy Wise,[1, *] A.A. Alemi,[1, †] R. Lundock,[1, ‡] G. Mueller,[1] D.H. Reitze,[1] D.B. Tanner,[1] and B.F. Whiting[1]

[1] *Department of Physics, University of Florida, P.O. Box 118440, Gainesville, FL 32611-8440, USA*
[2] *Department of Physics and Astronomy, University of Texas at Brownsville, 80 Fort Brown, Brownsville, TX 78520, USA*
(Dated: October 23, 2018)

Near-field radiative heat transfer allows heat to propagate across a small vacuum gap in quantities that are several orders of magnitude greater then the heat transfer by far-field, blackbody radiation. Although heat transfer via near-field effects has been discussed for many years, experimental verification of this theory has been very limited. We have measured the heat transfer between two macroscopic sapphire plates, finding an increase in agreement with expectations from theory. These experiments, conducted near 300 K, have measured the heat transfer as a function of separation over mm to μm and as a function of temperature differences between 2.5 and 30 K. The experiments demonstrate that evanescence can be put to work to transfer heat from an object without actually touching it.

Humans knew of radiative heat transfer at least as early as the discovery of fire, and physicists have investigated this process for centuries, culminating in the blackbody theory of Planck and the birth of the quantum theory. Planck's equation for black-body radiation contains only the temperature and some fundamental constants. When actual materials are involved, their emissivities enter the discussion, but little else. For example, the heat transfer per unit area between two semi-infinite planes is set by their temperatures and integrated emissivities but does not depend on their separation or other geometrical quantities. When the two planes approach each other closely the situation changes. In this near-field regime, each material interacts with exponentially decaying evanescent electromagnetic fields generated in and existing outside the other material; these fields can drive currents and generate heat.[1–3] This near-field radiative heat transfer can be several orders of magnitude greater than far-field blackbody radiation.

Much like the Casimir and van der Waals force, near-field heat transfer deals with fluctuations that only exist over small distances. The first in-depth theory for near-field heat transfer between planar surfaces was derived by Polder and Van Hove,[2] building on the work of Rytov[1]. There have been several other theoretical approaches, and in general the theory seems complete, except perhaps at distances comparable to atomic dimensions.[4]

Although heat transfer via near-field effects has been discussed for many years, experimental verification of the theory for heat transfer between two planar surfaces has been limited. Hargreaves[5] has presented room temperature observations for two Cr surfaces at distances as small as 1 μm. Domoto et al.[6] reported results at cryogenic temperatures but for relatively large (50 μm) separations, where near-field effects were barely observable. Neither study compared experiment to theory. A comparison at a fixed spacing has been put forward, but the plates were separated by polyethylene spacers, so the distance could not be varied.[7] There have also been several recent results using a sphere-plane geometry.[4, 7–9] There are engineering reasons for this approach, as, unlike a parallel plane geometry, a sphere-plane geometry needs no angular alignment. Using scanning probe and micro-machine technologies, these experiments cover a wide distance range.

In this paper, we report a set of measurements of heat transfer between two planar surfaces and present a detailed comparison to theory. In addition to its intrinsic interest, this work was motivated by possible applications in cooling objects without actually touching them, such as the mirrors of a future laser interferometer gravitational-wave detector.[10] This application would require the parallel plane geometry in order to get large areas of close approach of the two objects and thus significant heat transfer.

The near-field heat-transfer process can be thought of as a form of frustrated total internal reflection. Evanescent waves, exponentially-decaying electromagnetic fields, exist outside, but near to, the surface of a material medium at temperature T. These decaying fields are a consequence of travelling waves inside the medium experiencing total internal reflection; this phenomenon occurs when there is no valid solution to Snell's Law, $n_i \sin\theta_i = n_t \sin\theta_t$, where n_i and n_t are the indices of refraction and θ_i and θ_t the angle between wave vector and surface normal on the two sides of the interface. Although there is no energy transmission across the interface, an electric field exists on the far side. Furthermore, if another medium is brought near this exponentially decaying field some of the energy from the incident beam will propagate across the gap and into the new material. If one medium is hotter than the other, this photon tunneling will lead to heat transfer from hot to cold.

Polder and Van Hove[2] considered two half spaces of

identical material but different temperatures. The computed heat transfer coefficient $\mathcal{W}$ comes from the temperature derivative of the z component of the Poynting vector (S_z) from each medium, which is evaluated just inside surface of the other medium. $\mathcal{W}$ is the temperature derivative of this difference as can be seen in Eq. 1.

$$\mathcal{W} = \lim_{T_1 - T_2 \to 0} \left| \frac{S_z(d_+) - S_z(0_-)}{T_1 - T_2} \right| = \frac{\partial S_z(d_+)}{\partial T_1} \quad (1)$$

It is convenient to break $\mathcal{W}$ into two components

$$\mathcal{W} = \mathcal{W}_{\text{sin}} + \mathcal{W}_{\text{exp}}. \quad (2)$$

$\mathcal{W}_{\text{sin}}$ is the part where the wave number k_x of the field is in the range $0 < k_x < \omega/c$, where the field is propagating, and which gives the ordinary (Stefan-Boltzmann) far-field radiation. $\mathcal{W}_{\text{exp}}$ is the component where the field is exponentially decaying away from the surface; it is the larger contributor to the near-field limit:

$$\mathcal{W}_{\text{exp}} = \int_0^\infty d\omega \int_{\omega/c}^\infty dk_x \frac{k_x}{4\pi^2} (\mathcal{T}_\parallel^{\text{exp}} + \mathcal{T}_\perp^{\text{exp}}) \frac{\partial[\frac{\hbar\omega}{e^{\hbar\omega/kT}-1}]}{\partial T} \quad (3)$$

where the energy transmission coefficients are

$$\mathcal{T}_P^{\text{exp}} = \frac{1 - \cos(2\chi_P)}{\cosh[2\kappa(d - \delta_P)] - \cos(2\chi_P)}, \quad (4)$$

with $P = \parallel$ or $\perp$ for the two polarizations and $\chi_\parallel$ and $\chi_\perp$ being the phase shifts on reflection

$$\chi_\parallel = \arg[(-i\kappa\epsilon + k_z)(-i\kappa\epsilon - k_z)^*], \quad (5)$$

$$\chi_\perp = \arg[(-i\kappa + k_z)(-i\kappa - k_z)^*], \quad (6)$$

with ϵ the material dielectric function. $\delta_\parallel$ and $\delta_\perp$ can be derived from

$$e^{2\kappa\delta_\parallel} = \left| \frac{i\kappa\epsilon + k_z}{i\kappa\epsilon - k_z} \right|^2, \quad (7)$$

$$e^{2\kappa\delta_\perp} = \left| \frac{i\kappa + k_z}{i\kappa - k_z} \right|^2, \quad (8)$$

and k_z and κ are the z component of k for the medium and the vacuum, respectively

$$k_z = \sqrt{(\epsilon - 1)\omega^2/c^2 - \kappa^2}, \quad (9)$$

$$\kappa = ik_{zv} = \sqrt{k_x^2 - \omega^2/c^2}. \quad (10)$$

Note that $k_x > \omega/c$, so that k_{zv} is imaginary above the surface and the energy transmission coefficients $\mathcal{T}_\parallel^{\text{exp}}$ and $\mathcal{T}_\perp^{\text{exp}}$ are not derived from the energy reflection coefficients $\mathcal{R}_\parallel$ and $\mathcal{R}_\perp$.[2] We have used this theory to calculate the heat transfer coefficient between sapphire plates, using Barker's sapphire dielectric function.[11]
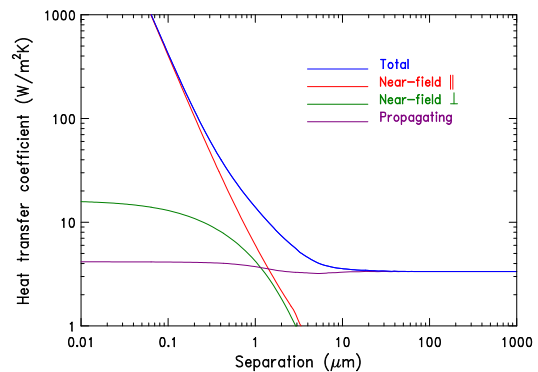

FIG. 1. Heat transfer coefficient vs. distance for z-cut sapphire. The temperatures of the two media are $T_{\text{hot}} = 310$ K and $T_{\text{cold}} = 300$ K, respectively. The violet curve shows $\mathcal{W}_{\text{sin}}^\parallel + W_{\text{sin}}^\perp$ which dominate at far distances. The red curve shows $\mathcal{W}_{\text{exp}}^\parallel$. The green curve shows $\mathcal{W}_{\text{exp}}^\perp$. The evanescent terms dominate at close distances. The blue curve is the total heat transfer coefficient $\mathcal{W}$.

Figure 1 shows the prediction of the model for z-cut sapphire; the temperatures of the two media are $T_{\text{hot}} = 310$ K and $T_{\text{cold}} = 300$ K. The $\mathcal{W}_{\text{sin}}$ term dominates at large separation and is nearly constant with separation. The $\mathcal{W}_{\text{exp}}$ term dominates in the near-field regime, so that the total heat transfer changes from being independent of separation at large distances towards $\mathcal{W}_{\text{exp}} \propto 1/d^2$ at short distances. The turning point between $\mathcal{W}_{\text{sin}}$ and $\mathcal{W}_{\text{exp}}$ occurs when the separation is approximately equal to the peak wavelength of the blackbody curve of the hot half space. Wien's displacement law predicts that $\lambda_{max} \approx 9$ μm when the temperature is 310 K.

A sketch of our apparatus is shown in Fig. 2. It is designed around two $50 \times 50 \times 5$ mm^3 sapphire plates. These have a specified flatness of $\lambda/8$ @ 633 nm per inch on the largest surfaces and are cut such that the c axis is perpendicular to these surfaces (z-cut). Sapphire was used because it has good thermal conductivity. It is also a candidate for the test masses of future gravitational-wave detectors.

One of the plates, henceforth called the cold plate, is attached to the thermal bath that is the vacuum chamber. The other plate, the hot plate, is thermally isolated from the bath by a Macor spacer attached to the back side of the hot plate. The hot plate also has a heater wound on a copper ring which is itself attached to the back of the plate. The heater current and voltage, after correcting for lead resistance, give the power required to maintain a given temperature difference between the hot and cold plates. Both plates have a Si-diode thermometer fastened to their backs to read the temperature (and for the hot plate to control it). Both plates have all four corners coated with an approximately 200 nm thick layer of sputtered copper. These coatings have areas about
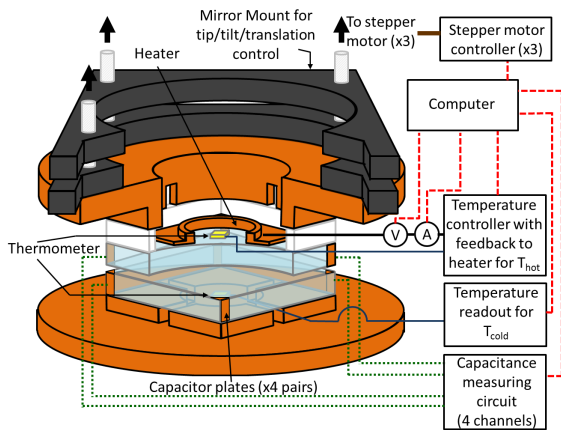
FIG. 2. Experimental apparatus. Stepper motors allow adjustment of the spacing, tip, and tilt (read capacitively) of two sapphire plates. The temperature of the hot plate is controlled by a feedback circuit, and the power required to maintain a temperature difference gives the heat transfer from the hot plate to the cold plate and to the thermal bath.

FIG. 3. Heat transfer coefficient vs. distance. The curves are each offset vertically by 2 W/m²·K from the one below. The points are the data, with error bars, determined from the scatter in the heat transfer measurements and the uncertainty in the distance calibration. The solid lines are the theoretical predictions for flat plates while the dashed lines are the theoretical predictions for slightly curved plates (see text). Each measured curve has a reproducible addendum due to other heat leaks which are not included in the model and which has been subtracted from the data. The temperatures are (top to bottom): $T_{\mathrm{hot}} = 327.0$ K, $T_{\mathrm{cold}} = 308.0$ K; $T_{\mathrm{hot}} = 322.0$ K, $T_{\mathrm{cold}} = 307.0$ K; $T_{\mathrm{hot}} = 317.0$ K, $T_{\mathrm{cold}} = 305.8$ K; $T_{\mathrm{hot}} = 312.0$ K, $T_{\mathrm{cold}} = 305.2$ K.

1 mm² and serve as capacitor plates that are read by four 24-bit capacitance-to-digital converter circuits[12] to measure the separation and angular misalignments of the plates. The metal film is wrapped around to the sides of the sapphire to allow electrical contact to the electrodes.

The cold plate is glued to a copper disk, which in turn is attached to the experimental structure. The Macor spacer on the back of the hot plate is attached to a modified kinematic mirror mount which allows for z-axis linear movement and tip and tilt angular adjustment by turning the three adjustment screws in the back. Three stepper motors turn screws on the kinematic mount via gear reduction boxes; each motor step translates to a linear movement of the hot plate by 35 nm. The components are held together by an "L" shaped backbone (not shown) to give rigidity. The assembly is located in a UHV chamber, with a base pressure below 2×10^{-7} Torr, making gas conduction negligible. Signals to the stepper motors, capacitance readouts, temperature readouts, and current and voltages to the heater are all controlled and/or read by a LabVIEW computer program.

Each pair of capacitor plates is calibrated by taking capacitance readings as the plates are driven together one step of the stepper motors at a time. A fit is made to $C = \epsilon_0 a/d + C_{\mathrm{stray}}$ where ϵ_0 is the dielectric constant of the vacuum, a is the capacitor area, and C_{stray} is a parallel contribution independent of separation. The data fits the equation above very well, with R^2 values greater than 0.999. The fitted value of a equals the metalized area within our knowledge of this area; $C_{\mathrm{stray}} \approx 0.4$ pF. The average capacitance gives the distance while the individual readings are used to correct the alignment by sending steps to the motors controlling tip and tilt.

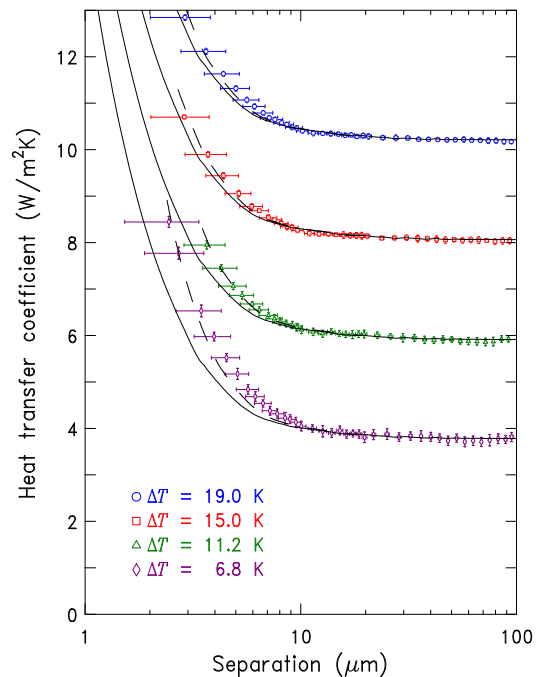To measure the heat transfer coefficient we compute

$\mathcal{W} = P/[A(T_{\mathrm{hot}} - T_{\mathrm{cold}})]$, where P is the power dissipated in the heater, A is the plate surface area, and T_{hot} and T_{cold} are the temperatures of the hot and cold plates, respectively. The data are a sum of parallel heat pathways, including thermal conduction through the Macor spacer and the other parts of the hot-plate holder, radiation to the thermal bath, and the contributions of the near- and far-field radiation between the two plates. We can observe the near-field effect because it is the only one of these that will change with plate separation. The thermal conduction and radiation-to-the-bath paths just add a constant offset to the radiative heat transfer that the model predicts.

Data for the heat transfer coefficient versus distance were collected for four temperature differences. (See Fig. 3.) Each one shows that near-field heat transfer exists and that the data and model agree reasonably well. Each run covers a separation range of about 2-100 μm. The only freedom in the fit is an offset to the model. All our measurements have an offset of 0.0435 ± 0.0004 W/K, completely consistent with thermal conduction through
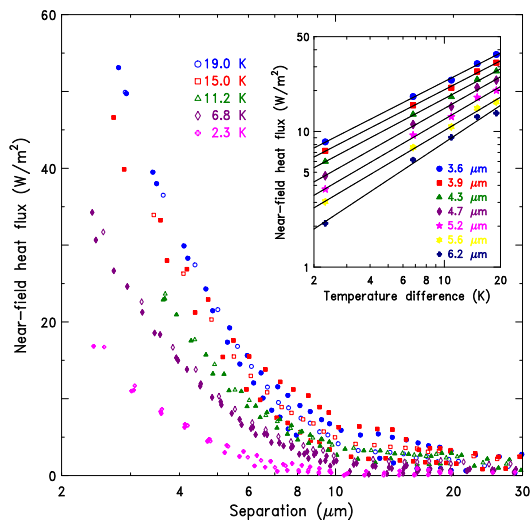
FIG. 4. Near-field heat flux vs. distance for multiple temperature differences and multiple runs. (One run is shown with open symbols and other runs with filled symbols.) The inset shows the near-field heat flux vs. temperature difference for several specific separation distances.

the Macor spacer and the rest of the support for the hot plate, in parallel with radiation from the rear surface of the plate. The chamber pressure for these runs ranged between 5×10^{-7} Torr and 2×10^{-7} Torr. The vacuum chamber is held at constant temperature of $30.0\,°\mathrm{C}$ (303.2 K). The hot plate is brought close to the cold plate step by step. Each datum is an average of a set of 500 values, in both heat transfer coefficient and distance, taken after the system has reached thermal equilibrium. It takes 30 to 45 minutes after moving to a new position to reach thermal equilibrium. We calculate the average and its standard deviation and plot these in Fig. 3.

Theoretical curves match the experimental data well. However, although the agreement is within experimental errors, there does appear to be a systematic offset: the theory predicts a slightly lower heat transfer coefficient at each separation than we measure. Alternatively, the plates could be slightly closer than measured by the capacitive readout. We believe that the latter explanation is correct. Simulations of the heat transfer between two convex plates (shown as dashed lines) eliminate the systematic error when the radius of curvature in each plate is ~1 km,corresponding to deviations from flatness of 500 nm. Subsequently, we measured the plate curvatures using optical flats and green mercury light; the Newton's rings interference pattern gave a central displacement of 170 ± 30 nm with respect to the perimeter, a little smaller but of the same order of magnitude as the simulation gave.

Figure 4 shows the heat flux caused by near-field effects. Both far-field heat transfer and the offset due to heat leaks to the thermal bath have been subtracted.

For each temperature difference, data are shown for several distinct data runs; these agree very well. The inset shows the dependence on the temperature difference of the plates. For distance values where the near-field effects dominate, the heat flux is linear in the temperature difference. Both data and model were fitted to

$$\phi(\Delta T, d) = G(d)\,(\Delta T)^{\alpha(d)} \tag{11}$$

where $\phi(\Delta T, d)$ is the total near-field heat flux, $G(d)$ is a multiplicative factor, and $\alpha(d)$ is the exponent for ΔT. Each curve follows a power law in ΔT, with the exponent varying from 0.70 at small distances to 0.91 at larger distances. The differential heat transfer, Eq. 1, has $\alpha(d) = 1$; the finite temperature differences used in the experiment bring in higher-order terms.

In summary we have measured near-field heat transfer across a small gap for a parallel-plane geometry. The data agree quite well with the theory of Polder and Van Hove[2]. The experiments demonstrate that significant amounts of heat can be transferred via evanescent radiation in the near-field regime.

* Current address: Department of Physics and Atmospheric Science, Dalhousie University, Halifax, NS B3H3J5, Canada

† Current address: Department of Physics, Cornell University, Ithaca, NY 14853-2501, USA

‡ Current address: Astronomical Institute, Tohoku University, Aoba, Sendai 980-8578, Japan

[1] S. Rytov, *Theory of Electric Fluctuations and Thermal Radiation* (Academy of Sciences Press, Moscow, 1953). Translation in AFCRC-TR-59-162 (1959).

[2] D. Polder and M. Van Hove, Phys. Rev. B **4**, 3303 (1971).

[3] Jackson J. Loomis and Humphrey J. Maris, Phys. Rev. B **50**, 18517 (1994).

[4] A. Kittel, W. Müller-Hirsch, J. Parisi, S.A. Biehs, D. Reddig, and M. Holthaus, Phys. Rev. Lett. **95**, 224301 (2005).

[5] C.M. Hargreaves, Phys. Lett. A **30**, 491 (1969).

[6] G.A. Domoto, R.F. Boehm, and C.L. Tien, J. Heat Transfer **92**, 412 (1970).

[7] A. Narayanaswamy, S. Shen, and L. Hu, Appl. Phys. A **96**, 357 (2009).

[8] E. Rousseau, A. Siria, G. Jourdan, S. Volz, F. Comin, J. Chevrier, and J. Greffet, Nature Photonics **3**, 514 (2009).

[9] S. Shen, A. Narayanaswamy, and G. Chen, Nano Lett. **9**, 2909 (2009).

[10] S. Wise, *Sensitivity Enhancement in Future Interferometric Gravitational Wave Detectors*, Ph.D. thesis, University of Florida, 2006. (unpublished)

[11] A. Barker Jr., Phys. Rev. **132**, 1474 (1963).

[12] Analog Devices, Inc., *AD7746: 24-Bit Capacitance-to-Digital Converter with Temperature Sensor* (2005).